Journal of Materials Chemistry B

ROYAL SOCIETY OF CHEMISTRY

PAPER

View Article Online
View Journal | View Issue

Cite this: J. Mater. Chem. B, 2025, 13, 14454

Supramolecular eutectogel based on THDESs as a skin penetrating carrier for effective transdermal delivery of hydrophobic drug curcumin

Nildhara Parsana,[a] Priyam Patel,[a] Hiral Ukani,[a] Sugam Kumar,[b] Vinod K Aswal,[b] Omar A. El Seoud[c] and Naved I. Malek *[ac]

Therapeutic hydrophobic deep eutectic solvents (THDESs) are an emerging class of eutectic mixtures gaining significant attention in the biomedical field. Solidifying these THDESs into bioactive eutectogels broadens their application in transdermal drug delivery (TDD). To showcase the potential of these sustainable materials, we have developed a supramolecular eutectogel within THDESs. The investigated eutectogels were formed by dissolving pharmaceutically active compounds, cetylpyridinium chloride (CPCl) and cetylpyridinium bromide (CPBr), in THDESs, which were formed by the interaction of menthol (Mth) with fatty acids (FAs) such as lauric acid (LA), palmitic acid (PA), and oleic acid (Ole) through hydrogen bonding. The resulting supramolecular eutectogels, which form solely *via* reversible noncovalent interactions in response to temperature, exhibit a sol–gel–sol transition, highlighting their reversible temperature responsiveness. Furthermore, these eutectogels remain stable at room temperature for approximately four months, with no alteration in their physical properties. Notably, the mechanical properties of these eutectogels vary according to the chain length of the FAs used to form the specific THDES, with longer chain lengths imparting greater mechanical strength, following the order (Mth + Ole-DES) MeOle > (Mth + PA-DES) MePA > (Mth + LA-DES) MeLA. These eutectogels also show excellent adhesive properties on various substrates, including skin. Moreover, they retain the bioactivity of the THDESs and enhance skin penetration, facilitating the delivery of the anticancer drug curcumin in an *ex vivo* goat skin model *via* a Franz diffusion cell. These eutectogels exemplify the relationship between the system's hydrophobicity and its influence on curcumin loading capacity and skin permeation ability, paving the way for the development of innovative therapeutic soft materials.

Received 19th June 2025,
Accepted 28th September 2025

DOI: 10.1039/d5tb01470k

rsc.li/materials-b

1. Introduction

Curcumin, a polyphenol found in the rhizome of *Curcuma longa* (turmeric), is an α,β-unsaturated diketone (diferuloylmethane) known for its keto–enol tautomerism. Traditionally used in medicine for its health benefits, curcumin exhibits antioxidant,[1] anti-inflammatory,[2] anti-microbial,[3] anti-cancer,[4] nephroprotective,[5] and anti-diabetic[6] properties. Among its diverse pharmacological properties, the anti-cancer properties of curcumin have gained considerable interest in the past five decades. Studies have demonstrated its ability to inhibit tumor formation[7–9] and progression[10–12] in various animal models of carcinogenesis. Recent clinical trials focusing on patients with familial adenomatous polyposis have further supported its potential in reducing cancer progression across multiple organ sites, thereby positioning it as a promising agent for both cancer prevention and treatment.[13] However, curcumin's poor aqueous solubility, low bioavailability, and susceptibility to gastrointestinal degradation limit its therapeutic application.[14] To address these limitations and enhance its therapeutic efficacy, higher doses of curcumin (12 to 20 grams daily) are often recommended, which consequently increase the risk of side effects like gastrointestinal irritation.[15,16] Therefore, developing new drug delivery systems is crucial for enhancing its therapeutic efficacy and minimizing side effects, particularly through the use of simple solvents to bypass expensive and time-intensive processes. This necessitates the exploration of new solvents that offer enhanced solubility of the active compound while ensuring environmental and health safety. In this

[a] Ionic Liquids Research Laboratory, Department of Chemistry, Sardar Vallabhbhai National Institute of Technology, Surat-395007, Gujarat, India. E-mail: navedmalek@chem.svnit.ac.in
[b] Solid State Physics Division, Bhabha Atomic Research Centre, Trombay, Mumbai-400085, India
[c] Institute of Chemistry, University of São Paulo, 05508-000 São Paulo, SP, Brazil

regard, ionic liquids (ILs) and deep eutectic solvents (DESs) have emerged as a particularly intriguing group of solvents. For instance, Goto's group improved curcumin's solubility to ~8 mg mL^{-1} and extended its half-life to 260 minutes by encapsulating it within the [Ch][Ole] IL.[17] Similarly, our previous work demonstrated that DES-based eutectogels can solubilize 42–45 mg g^{-1} of curcumin,[18] and Jeliński *et al.* showed that a DES of choline chloride and glycerol (1 : 1) dissolves up to 7.25 mg mL^{-1} of curcumin.[19] These findings underscore the superior drug solubilizing capacity of DESs. Furthermore, DESs offer additional benefits over conventional ILs, including minimal toxicity, cost-efficiency, simple preparation and handling, justifying our focus on DES-based solutions.

Having shown promise in the field of biomedical applications, DESs find utility in enhancing the solubility, skin penetration, and absorption of active pharmaceutical ingredients (APIs).[20] These APIs can themselves serve as counterparts to DESs, forming what are referred to as therapeutic deep eutectic systems (TDESs).[21,22] This study aims to provide insights into the therapeutic hydrophobic DES (THDES) formulated with menthol (Mth) and various fatty acids (FAs). Although FA-based THDESs have been previously reported in the literature, primarily for purposes such as wastewater treatment, bioelectronics, enzyme activation, microalgal biomass and plant material extraction, as well as antibacterial and wound healing applications, there is a scarcity of literature regarding eutectogel formulations based on these THDESs for TDDSs, leaving ample space for innovative biomedical materials. Mth with its extremely low solubility in water (0.46 mg mL^{-1} at RT) and effectiveness as a skin penetration enhancer (PE) along with its established anti-inflammatory and antimicrobial characteristics has emerged as an ideal candidate for designing sustainable and cost-effective THDESs.[23] On the other hand, FAs are frequently derived from plant and animal fats, and their strong antimicrobial properties have also been reported.[24,25] The European Food Safety Authority (EFSA) has published an opinion regarding FAs as food additives, stating that they are deemed safe at the generally recognized as safe (GRAS) level.[26] They also play a significant role in the natural self-disinfection process of human skin.[24] Therefore, even if they penetrate the skin, their biocompatibility suggests they may not induce skin inflammation.[27] Thus, these FA-based THDESs for TDD are anticipated to act as PEs without causing skin irritation. When THDESs form supramolecular eutectogels solely *via* reversible noncovalent interactions, they present an appealing choice for biomedical applications. Due to the involvement of noncovalent interactions, these gels frequently exhibit stimulus-responsive and self-healing characteristics. Moreover, their gel phase prolongs contact with the skin, facilitating sustained and controlled drug release in TDDSs. To the best of our knowledge, no studies have yet explored the application of Mth-FA THDES-based supramolecular eutectogels in TDDSs.

In our pursuit to develop nanocarriers with biocompatible features such as IL-based micelles-vesicles,[28] hydrogels[29,30] and aerogels[31] here we present the development of supramolecular eutectogels. The proposed eutectogels are developed by self-assembling the two long-chain surfactants CPCl and CPBr in the THDESs comprising of Mth and FAs, *i.e.*, LA, PA and Ole, through intermolecular non-covalent bonds. Fig. 1(i) illustrates the structures of the components used in the preparation of the eutectogels. These eutectogels offer several advantages, including simple preparation and handling, skin penetration capability, biocompatibility, and stimuli-responsiveness. This study focuses on curcumin as a model hydrophobic drug due to its known transdermal delivery limitations; however, the developed eutectogel platform is expected to be applicable to other poorly soluble hydrophobic drugs in future studies.

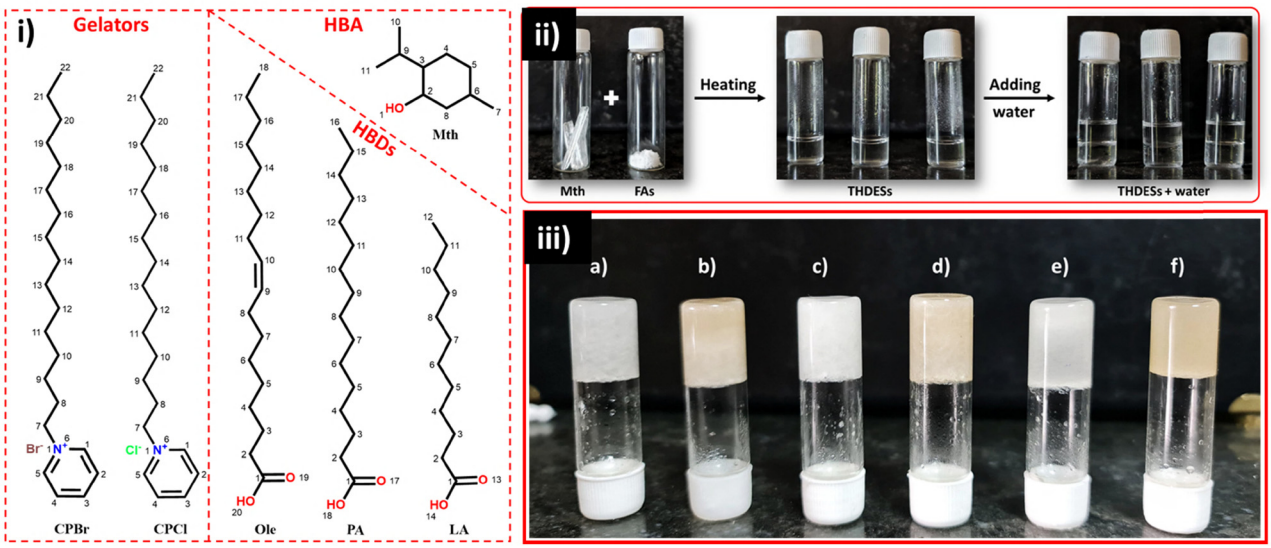

Fig. 1 (i) Chemical structures of components; (ii) formation of THDESs and phase separation with water; (iii) visual representation of eutectogel formation by vial inversion: (a) **MeLA-CPCl**, (b) **MeLA-CPBr**, (c) **MePA-CPCl**, (d) **MePA-CPBr**, (e) **MeOle-CPCl**, and (f) **MeOle-CPBr**.

2. Experimental section

2.1. Materials

L-Menthol was acquired from Sigma-Aldrich), lauric acid from TCI Chemicals), palmitic acid from Merck, and oleic acid, cetylpyridinium chloride, cetylpyridinium bromide, and curcumin from SRL. All chemicals were of reagent grade and used as received without additional purification.

2.2. Methods

2.2.1. General preparation of THDESs. The THDESs used in this study were prepared according to the established procedure.[32–34] In summary, the HBA (Mth) and HBDs (LA, PA, Ole) were mixed in a specific molar ratio outlined in Table 1. Subsequently, the mixture was heated using a magnetic stirrer until a homogeneous solution was formed (~70 °C). The resultant DESs, devoid of discernible fine particles and air bubbles, were then stored in a sealed container at room temperature. Fig. 1(ii) demonstrates the formation of hydrophobic THDESs. The observed difference in required ratios to form THDEDs arises from the physicochemical properties of the used FAs. PA (C16 : 0) is highly crystalline, with a higher melting point and stronger van der Waals interactions compared to lauric acid (C12 : 0), hence requiring a larger excess of menthol to sufficiently disrupt its lattice. In contrast, oleic acid (C18 : 1, *cis*) contains a double bond that introduces a kink in the chain, lowering its melting point and disrupting crystalline packing. This enhances miscibility with menthol and favors near-equimolar association (1 : 1), allowing MeOle to form a stable THDES without requiring a large excess of menthol. Thus, the ratios reflect the balance between chain length, saturation, and molecular packing of the fatty acids rather than a simple chain-length trend.

2.2.2. General preparation of eutectogels. Six eutectogels were prepared by a simple one-step hot dissolution/cooling process. Specific amounts of surfactants (CPCl or CPBr) were added to THDESs in a sample vial, and the mixtures were heated in a water bath at 60–65 °C until a clear transparent solution was obtained. The vials were then cooled to room temperature, resulting in the formation of eutectogels. Gel formation was evaluated using the vial inversion method (Fig. 1(iii), a–f) and the falling ball method (Video S1). To optimize the composition, different concentrations of CPCl and CPBr were tested. We found that at 3% w/v concentration, both surfactants consistently produced stable eutectogels with non-flowing properties, whereas at concentrations below 3% the system remained in the sol state. From an economical perspective, the minimum concentration of 3% was therefore selected and used in all further studies (Table 1).

The use of both CPCl and CPBr was intentional, as halide counterions are known to influence the self-assembly and physicochemical behavior of quaternary ammonium surfactants. We initially anticipated that differences in ionic radius and hydration between chloride and bromide could affect gelation, stability, or drug loading. Although the outcomes were comparable, this comparison suggests the robustness of the eutectogel platform, which performs effectively irrespective of the counterion.

2.2.3. FTIR. FTIR spectra for Mth and associated fatty acids (LA, PA, Ole) were obtained using a Shimadzu FT-IR-8400S spectrophotometer with KBr pellets (1 wt% sample), in the range of 400–4000 cm^{-1}. The establishment of hydrogen bonding between the HBD and HBA to form a THDES was inferred from the FTIR spectra by comparing the spectra of individual components with the spectra of their respective THDES. Additionally, the eutectogels were also subjected to FTIR analysis to investigate the interactions accountable for gel formation, following a similar procedure.

2.2.4. SANS. SANS analysis of representative eutectogels (**MeLA-CPBr**, **MePA-CPBr** and **MeOle-CPBr**) from each THDES (MeLA, MePA and MeOle) was conducted using a SANS-1 diffractometer at the Guide Tube laboratory, Dhruva reactor, BARC, Mumbai, India. The experimental data were analyzed with SasView software, employing various fitting models. The sample data were fitted using an empirical functional form for SANS data, characterized by a broad scattering peak. The scattered intensity, $I(q)$, is calculated using the following eqn (1):[35,36]

$$I(q) = \frac{A}{q^n} + \frac{C}{1 + (|q - q_0|\xi)^m} + B \quad (1)$$

The first term accounts for scattering observed in the low-q range, which provides information from larger objects in the

Table 1 Molar ratios of individual components used for DES formation and composition of surfactants for eutectogel formation, along with their abbreviations as used in the manuscript

THDES	HBA	HBD	Molar ratio (HBA : HBD)	Gelator	Gelator (% w/v)	Observation
MeLA	Menthol (Mth)	Lauric acid (LA)	4 : 1	CPCl	1–2%	Sol
					3%	Gel (**MeLA-CPCl**)
				CPBr	1–2%	Sol
					3%	Gel (**MeLA-CPBr**)
MePA		Palmitic acid (PA)	12 : 1	CPCl	1–2%	Sol
					3%	Gel (**MePA-CPCl**)
				CPBr	1–2%	Sol
					3%	Gel (**MePA-CPBr**)
MeOle		Oleic acid (Ole)	1 : 1	CPCl	1–2%	Sol
					3%	Gel (**MeOle-CPCl**)
				CPBr	1–2%	Sol
					3%	Gel (**MeOle-CPBr**)

sample, while the second term, which describes a broad peak, reflects the inner structure of the objects and conveys information on the average separation between scattering inhomogeneities within the eutectogel network. Parameters A and C are multiplying constants that weight the contribution of each term (power law and broad peak) to the total scattering, while B is an additive constant that accounts for incoherent scattering. The exponent n provides information on the fractal dimensionality of objects, while the exponent m provides information on solvation. Additionally, q_0 indicates the interference peak position, which can be used to retrieve the average separation through the Bragg law, $d = 2\pi/q_0$. Parameter ξ represents the correlation length, which represents the degree of order in the structure: the higher the value of ξ, the greater the correlation between inhomogeneities in the inner structure.

2.2.5. SEM. The SEM images of the supramolecular eutectogel were obtained using a Hitachi S-3400N scanning electron microscope operating at 15 kV. The samples were affixed to a copper disc using double-sided carbon tape, and a layer of gold coating was applied to the gel samples.

2.2.6. Turbidity measurements. Turbidity measurements of each eutectogel were conducted using a Varian Cary 50 UV spectrophotometer, recording changes at a wavelength of 500 nm over time within the temperature range of 30–70 °C. For standard measurements, samples were introduced into a quartz cuvette, and spectra were recorded until the gel formation became apparent. Subsequently, the gel phase, observed at the end of the measurement, exhibited stability during the tube (cuvette) inversion test. The measurements are performed in triplicate to ensure accuracy.

2.2.7. Rheology. A Physica MCR 301 rheometer was employed for rheological measurements. Frequency scans were conducted over the range of 0.01–100 rad s^{-1} under a fixed strain of 0.25%. Additionally, strain scans were performed at a constant frequency of 1 rad s^{-1}, spanning from 0.01 to 10%. The point at which G' begins to deviate from linearity and eventually intersects with G'', leading to gel breakdown, corresponds to the critical strain.

2.2.8. Drug loading. For the curcumin encapsulation, initially, the eutectogels were subjected to heating beyond their Tgel temperature, followed by gradual cooling to room temperature. Just prior to the beginning of the transformation of the sol phase into the gel phase, curcumin was introduced into the sol phase at a temperature ranging between 30 and 35 °C, with an initial concentration of 25 mg mL^{-1}. During this phase, a portion of the curcumin solubilized while the remainder settled at the bottom of the vial. Following the sol-to-gel transition, curcumin became entrapped within the gel phase, with some residual curcumin remaining in the settled portion. To measure loading efficiency, a predetermined quantity of eutectogel was collected and dissolved in a known quantity of methanol, carefully avoiding inclusion of settled curcumin. The loading efficiency was subsequently quantified using UV-vis spectroscopy by comparing the absorbance with a standard calibration curve.

2.2.9. Drug permeation study. Whole-thickness goat skin from the ear pinna was collected for the investigation. Non-dermatome skin was excised using a scalpel after being cleaned with cold tap water. For skin permeation studies, a Franz diffusion cell was utilized, with an effective diffusion zone of 7.85 mm^2. In the receptor chamber, 10 ml of pH 7.4 PBS (30% PEG 400 v/v) was added and stirred using a magnetic stirrer (250 rpm). The temperature of the receptor chamber was maintained at 32 ± 1 °C with the assistance of an external constant temperature circulator water bath. The stratum corneum (SC) layer of the skin faced the donor chamber, situated between the donor and receptor compartments of the Franz diffusion cell. Next, curcumin-loaded eutectogels (500 μg g^{-1}) were introduced into the donor compartment, maintaining continuous contact with the SC for 48 h. Samples (1.0 mL) from the receptor chamber were collected at specified intervals, ensuring the maintenance of the sink state by replacing them with an equivalent amount of fresh buffer solution.

The cumulative amount of drug permeated per unit area (Q, μg cm^{-2}) was plotted against time (t, h). The steady-state flux (J, μg cm^{-2} h^{-1}) was obtained from the slope of the linear portion of the plot according to

$$J = \frac{dQ}{dt}$$

The permeation coefficient (K_p, cm h^{-1}) was calculated using the equation

$$K_p = \frac{J}{C_0}$$

where Q = cumulated amount of drug permeated per unit area (μg cm^{-2}), t = time, J = steady-state flux (μg cm^{-2} h^{-1}), K_p = permeability coefficient (cm h^{-1}) and C_0 = initial drug concentration in the donor compartment (μg cm^{-3})

2.2.10. Effect of eutectogels on the SC layer of skin (permeation mechanism). Following the drug permeation experiment, goat skins were removed from the Franz diffusion cell and carefully cleansed with methanol and water, followed by thorough drying. Subsequently, ATR-FTIR spectroscopy was employed to examine the impact of eutectogel on the lipid and keratin composition of the skin. The stratum corneum (SC) layer of the skin was placed facing downward onto the surface of the ATR crystal, and spectra were recorded within the range of 4000–400 cm^{-1} using a Jasco FTIR-ATR spectrophotometer.

2.2.11. Cytotoxicity assessment of eutectogels. We evaluated the biocompatibility of each eutectogel with human keratinocyte (HaCaT) cells using the MTT cell viability assay. HaCaT cells were thawed at 37 °C after being stored at −80 °C. Upon thawing, the old cell culture medium was replaced with fresh medium following centrifugation, and a cell suspension was prepared. This suspension was then transferred to a T-25 culture flask containing 5 mL of fresh media and incubated at 37 °C with 4% CO_2 until sufficient cell growth was achieved, forming a monolayer. Afterward, the monolayer was rinsed with PBS and disrupted by treatment with trypsin–EDTA solution for 2 minutes. The trypsin's action was halted by adding fresh media, and the solution was then centrifuged.

The suspended cells were mixed with fresh media and transferred to a T-75 culture flask for further growth. These cells were subsequently seeded into a 96-well plate to assess the cytotoxicity of the eutectogel using the MTT assay. Cell viability was determined by measuring absorbance at 570 nm with a microplate reader after 48 hours.

To evaluate the efficacy of the studied eutectogels against A431 human epidermoid carcinoma cells, the following procedure was employed. A431 cells were cultured in 10% complete media, comprising a mixture of fetal bovine serum and Dulbecco's minimal essential media, and maintained at 37 °C in a humidified atmosphere using a carbon dioxide incubator (Eppendorf CellXpert) until they reached confluency. Subsequently, the cells were exposed to increasing concentrations of eutectogels containing curcumin (5, 10, 15, 20, and 25 μM), along with eutectogels devoid of curcumin. After a 48-hour incubation period, the culture medium was carefully aspirated, and the cells were thoroughly washed with PBS buffer. The cells were then incubated for an additional 4 hours in fresh MTT media (2 mg mL^{-1}). Following the removal of the MTT media, 100 μL of DMSO was added to each well, and the plates were incubated at 37 °C for approximately 10 minutes to ensure complete solubilization. Subsequently, the absorbance of the resultant solution in each well was measured using a microplate reader.

2.2.12. Skin compatibility test. The skin compatibility of the representative eutectogels from each THDES (*i.e.*, **MeLA-CPBr**, **MePA-CPBr** and **MeOle-CPBr** gels) was assessed through a primary skin irritation test conducted on human volunteers. Six healthy volunteers of both genders, aged between 18 and 40 years, were selected. The exclusion criteria for the study included the presence of skin marks or lesions in the test area that could interfere with the assessment, a history of eczematous conditions, allergy or sensitivity to the components being tested, dermographism, increased skin reactivity, atopy, allergy to adhesives, recent use of topical corticosteroids in the test area, pregnancy, lactation, or ongoing treatment with anti-inflammatory or antiallergic medications.[37] For each of the three eutectogels, two volunteers were assigned per formulation. A 1.0 g sample of the eutectogel was applied to a 2-square-inch area on the back of the hand for up to 4 hours. The treatment sites were then evaluated for any signs of irritation or redness using a four-point grading scale (Table S1) proposed by the International Contact Dermatitis Research Group (ICDRG) at 24, 48, and 72 hours post treatment.[38] Informed consent was obtained from all volunteers prior to their participation in the experiments.

3. Results and discussion

The THDES-based supramolecular eutectogels were prepared by dissolving CPCl and CPBr at the concentrations listed in Table 1 within each of the THDESs. Their formation was first confirmed using FTIR, which verified both the successful preparation of the THDESs and the subsequent supramolecular eutectogels. To further support this, SANS measurements were carried out, confirming the presence of aggregates in the THDESs that drive eutectogel formation. In FTIR analysis, the FTIR spectra of the THDESs were compared with those of the individual components (Mth, LA, PA, and Ole). As a representative system, the obtained spectra for the MeLA THDES and its corresponding components are shown in Fig. 2a and b, while additional spectra for other systems are provided in the SI (Fig. S1a–d). The components used as a HBD to form DESs have a carboxylic acid group in their structure, displaying a distinctive band (ketone or carbonyl group) at ~1700 cm^{-1} in their spectra. Conversely, the HBA, Mth, exhibits a characteristic band at ~3224 cm^{-1}, indicating the presence of the -OH group in its structure. Additionally, FTIR spectra of DESs showed intermolecular hydrogen bonding between HBDs and Mth, mostly in the carboxyl group region.[39] In Fig. 2a, the carbonyl band at ~1683 cm^{-1} in LA is shifted to ~1708 cm^{-1} in the MeLA DES. This significant change strongly indicates the formation of a new hydrogen bond, playing a crucial role in the formation of the DES. This was further supported by the physical state of the components. For instance, in the case of MeLA (DES) composed of Mth and LA, both individual compounds were initially in a solid state. However, after DES formation, a stable liquid state was achieved, indicating the establishment of hydrogen bonding between them.

The gelation of these DESs occurred through the addition of surfactants, driven by noncovalent interactions such as hydrophobic interactions, hydrogen bonds, and van der Waals forces. This was confirmed by comparing the FTIR spectra of powder CPCl and CPBr with the spectra of their corresponding eutectogels. For instance, we compared **MeLA-CPCl** and **MeLA-CPBr** gels with the MeLA DES, and CPCl, CPBr surfactants, respectively (Fig. 2b). The frequencies associated with the asymmetric and symmetric vibration of the $-CH_2$ group in CPCl (2960, 2894 cm^{-1}) and CPBr (2947, 2881 cm^{-1}) are shifted to 2909, 2843 cm^{-1} in the **MeLA-CPCl** gel and to 2906, 2840 cm^{-1} in the **MeLA-CPBr** gel, due to the hydrophobic interaction between the alkyl chains of surfactants. The interaction of DES molecules with the surfactant in the eutectogel is evident from the –OH stretching frequency which is shifted from 3343 cm^{-1} in the MeLA DES to 3329 cm^{-1} in the **MeLA-CPCl** gel and to 3330 cm^{-1} in the **MeLA-CPBr** gel (Fig. 2b). Similarly, FTIR analysis of the remaining eutectogels was conducted and is presented in the SI, Fig. S1b and d. The observed shifts in frequencies associated with the interactions between alkyl chains are crucial, as they indicate that the surfactants are self-assembling within the DES to form aggregates, leading to eutectogel formation. This important finding prompted us to conduct further studies using SANS analysis to confirm the formation of aggregates within the DES. As illustrated in Fig. 2c, the experimental SANS curves for the representative eutectogels—**MeLA-CPBr**, **MePA-CPBr**, and **MeOle-CPBr**—align well with the broad peak model. According to this model, the Lorentzian parameters are primarily derived from the higher Q region and are applicable when a broad scattering peak,

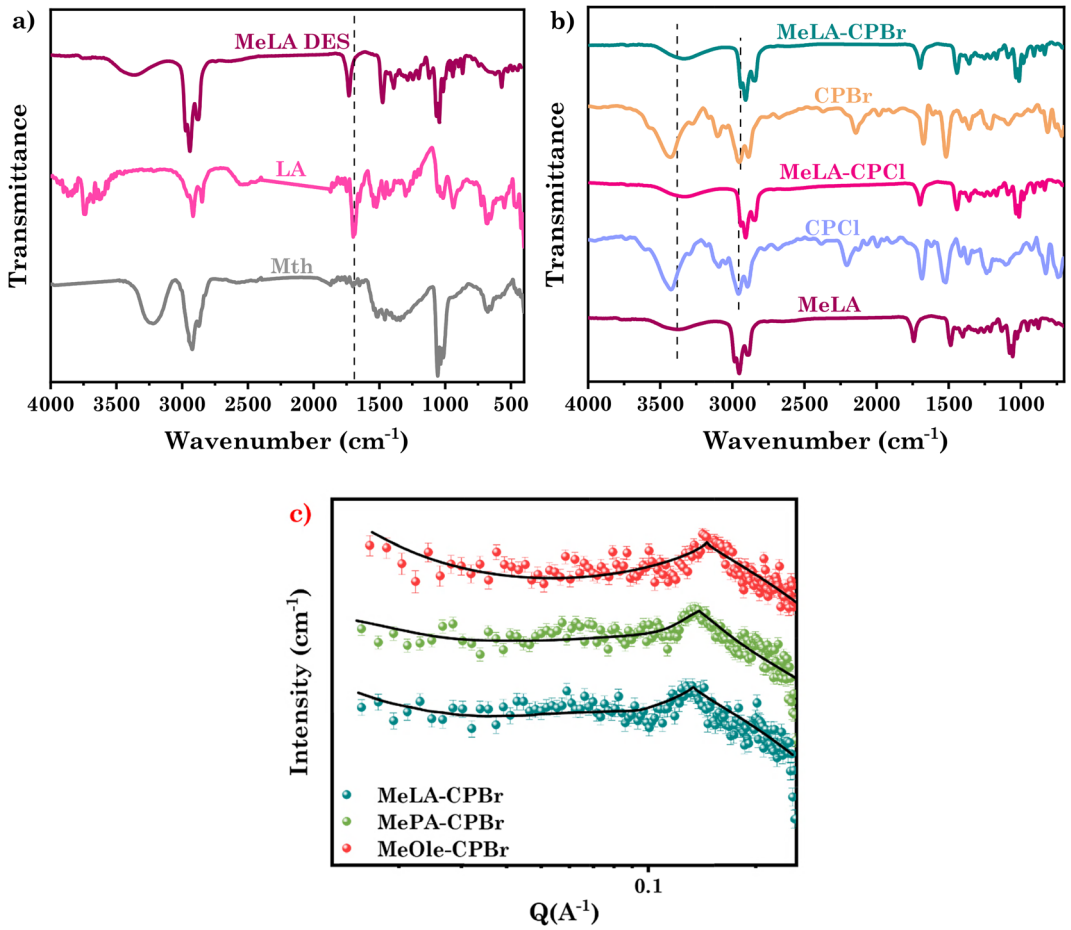

Fig. 2 FTIR spectra of (a) individual components (Mth, LA) in comparison with the spectra of their respective DES (MeLA) and (b) individual surfactants (CPCl, CPBr), DES (MeLA), and their corresponding gels (**MeLA-CPCl** and **MeLA-CPBr**); and (c) SANS data of representative eutectogels **MeLA-CPBr**, **MePA-CPBr** and **MeLA-CPBr** at 298.15 K.

resulting from interactions between aggregates, is present in the data. The Porod exponents obtained from the fitting parameters were found to be 1.4 for **MeLA-CPBr**, 1.3 for **MePA-CPBr**, and 1.0 for **MeOle-CPBr**. These values suggest elongated assemblies arranged into a network of branched fibers within the gel structure.[40] Furthermore, the correlation lengths, representing the average distance between aggregates, were found to be 45.31 Å for **MeLA-CPBr**, 43.35 Å for **MePA-CPBr**, and 40.05 Å for **MeOle-CPBr**. The higher hydrophobicity of **MeOle-CPBr** leads to enhanced hydrophobic interactions, which tend to result in more closely packed structures. The observed lower correlation length of the **MeOle-CPBr** system indicates that the average distance between aggregates is reduced, meaning the aggregates are slightly more closely spaced compared to the other two systems. All parameters of the fitting models are summarized in Table 2.

To further investigate the morphology and gain a better visual understanding of the structure of the studied eutectogels, we performed SEM analysis on the representative eutectogels (**MeLA-CPBr**, **MePA-CPBr**, and **MeOle-CPBr**) derived from three distinct DESs (MeLA, MePA and MeOle). The result revealed a distinctive 3-dimensional network structure (Fig. 3). Such morphology could be attributed to the gelator (CPCl and CPBr), which

Table 2 SANS fitting parameter of representative eutectogels

		Parameters			
S. no.	Eutectogel	Peak position (Å^{-1})	Correlation length (Å)	Porod exponent	χ^2
1	**MeLA-CPBr**	0.1292	45.31	1.4	1.2
2	**MePA-CPBr**	0.1395	43.35	1.2	1.3
3	**MeOle-CPBr**	0.1456	40.05	1.0	1.1

formed fiber-like aggregates. These aggregates are long enough to intertwine and overlap with each other, thereby promoting the formation of the observed eutectogel morphology. These results correspond with the SANS data showing lower correlation lengths for the **MeOle-CPBr** system, indicating a close spacing of aggregates. This close arrangement supports the formation of a slightly dense gel morphology, as seen in the SEM images, highlighting the role of hydrophobic interactions in network formation.

3.1. Thermal stability and opacity measurement of supramolecular eutectogels

The investigated eutectogels were expected to demonstrate temperature responsiveness owing to their noncovalent interactions as

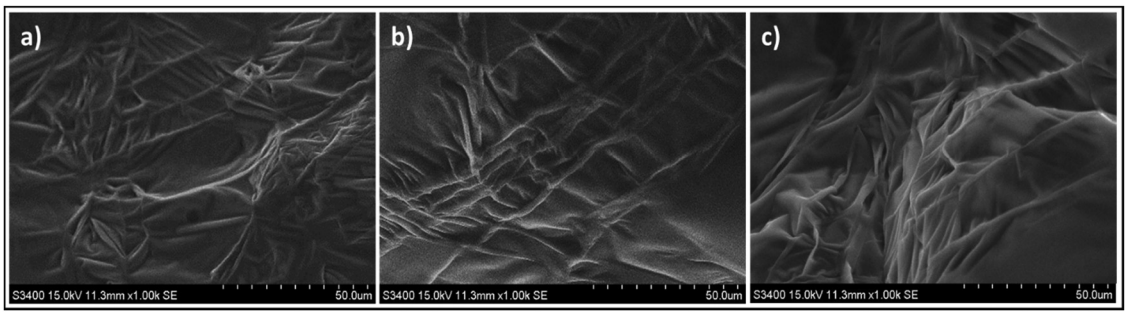

Fig. 3 SEM images of eutectogel (a) **MeOle-CPBr**, (b) **MePA-CPBr** and (c) **MeLA-CPBr** (1.00k× magnification; 15.0 kV HV; scale bar = 50 μm).

inferred from the FTIR spectra (*vide supra*), which leads to the association and dissociation of non-covalent interactions with the change in temperature. To investigate this phenomenon, particularly the temperature at which the gel-to-sol transition occurs (Tgel), we utilized the falling ball method, and the findings are outlined in Fig. S2. There is a limited temperature range difference in the thermal stability of all the eutectogels, roughly 8 °C from the lowest to the highest values. The transition from gel to sol could be attributed to the disintegration of the gel network with increasing temperature. In response to a decrease in temperature, the sol-to-gel transition was consistently observed in all cases, as evident in Video S1, thereby emphasizing the reversible temperature responsiveness of these materials. Furthermore, it is noteworthy that the supramolecular eutectogels exhibit sustained stability for ~4 months at RT, with no impact on their physical properties.

To assess the gelation kinetics, we quantified the opacity of the supramolecular eutectogels over time. Upon heating the gel beyond its Tgel (Video S1), it transforms into a sol state (transparent). Conversely, upon cooling to RT, the material reestablished the gel state and became opaque. To elucidate the gelation time, we monitored the opacity of each eutectogel at various time intervals. Our observation revealed that gelation occurs as a one-step process, and the duration required to reach the plateau is considered as the time for complete gelation. Among the studied systems, we noted that the MeOle-based system exhibited a slight rapid transition from sol to gel in comparison to the MeLA- and MePA-based eutectogels, as shown in Fig. 4a and b. This difference in gelation rates could be attributed to structural unsaturation in oleic acid, a key component of the DES (MeOle). This unsaturation imparts increased hydrophobicity, resulting in the increased hydrophobic interactions with the surfactants. These increased interactions contribute to a slightly more accelerated gelation process in the MeOle-based system when compared with the MeLA- and MePA-based eutectogels.

3.2. Mechanical properties of supramolecular eutectogels through rheology

The eutectogels were subjected to strain sweep and angular frequency sweep measurements to investigate their mechanical strength. Fig. 5c and d represent the change in the storage modulus (G') and loss modulus (G'') with angular frequency for each eutectogel. Remarkably, under a constant strain of 0.25%, G' consistently exceeded G'' throughout the whole frequency range for all investigated systems. This finding suggests the presence of a stable gel network within this frequency range. Further, we conducted strain sweep experiments at a fixed angular frequency of 1 rad s^{-1} to investigate the linear viscoelastic region (LVR) of the eutectogels. In all eutectogels initially, the gel samples displayed a higher G' than G'' as can be seen in

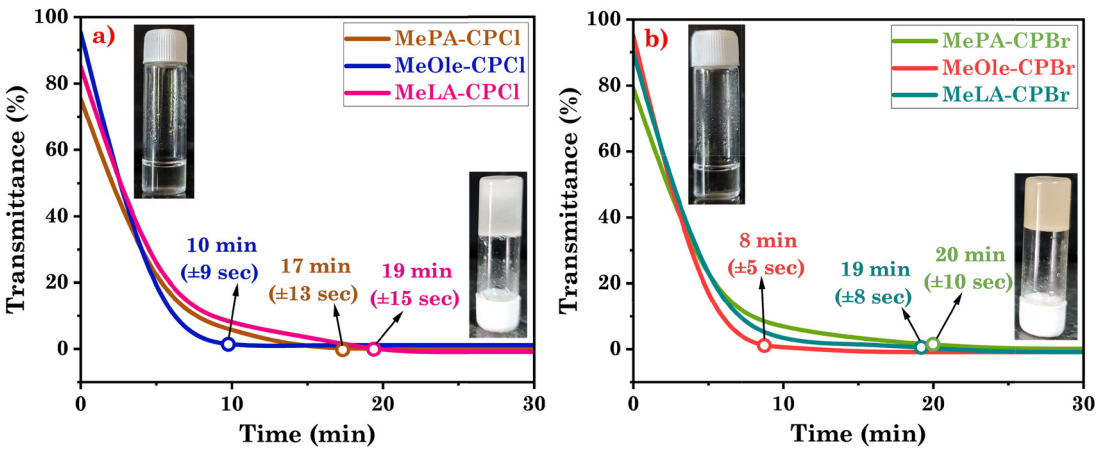

Fig. 4 Opacity measurement through transmittance measurement as a function of time for (a) **MeLA-CPCl**, **MePA-CPCl**, and **MeOle-CPCl** and (b) **MeLA-CPBr**, **MePA-CPBr**, and **MeOle-CPBr**.

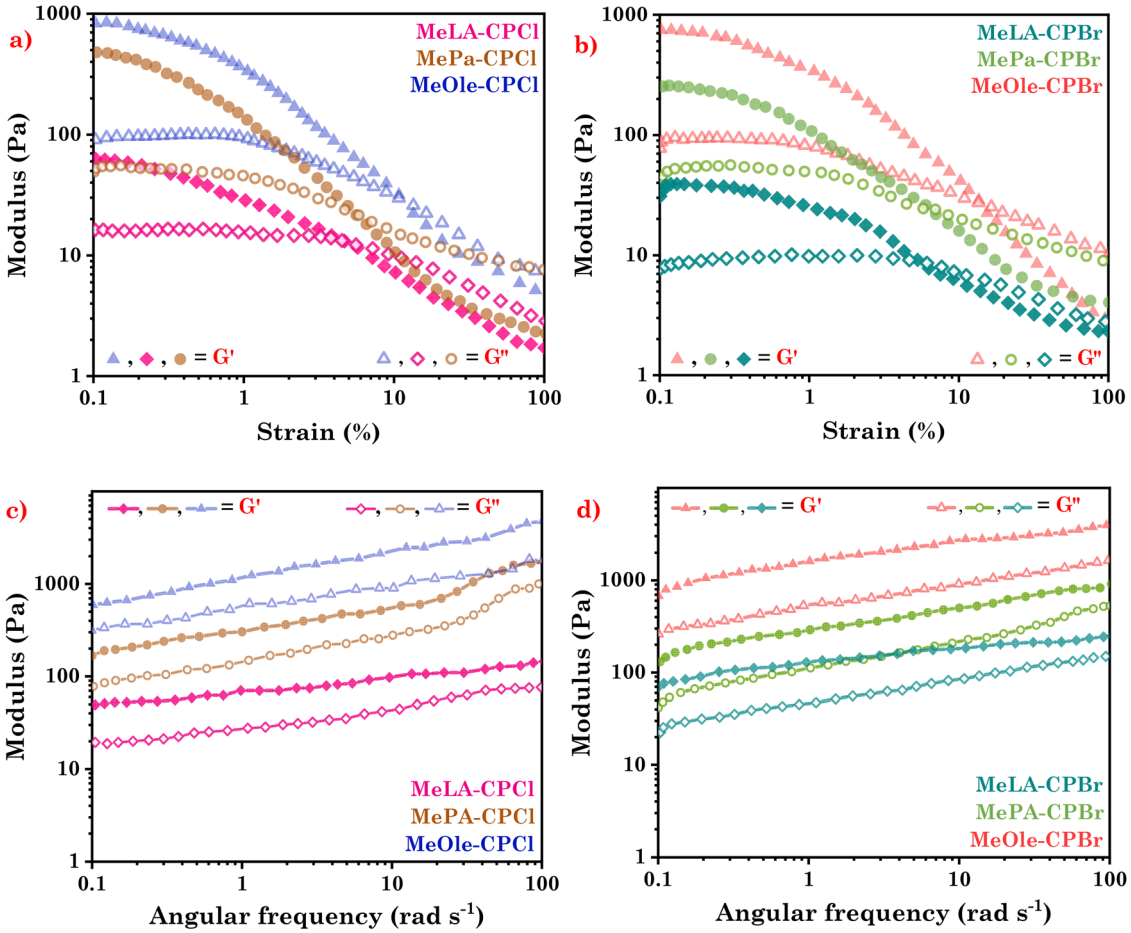

Fig. 5 Rheological study: (a) and (b) strain sweep measurement and (c) and (d) frequency sweep measurement.

Fig. 5a and b, indicating their gel-like behavior during the strain sweep analysis. For the MeOle based eutectogel, we observed that the values of G' and G'' remained independent of frequency up to ~12% strain, suggesting that the gel was within the LVR with consistent elasticity and viscosity. Beyond this strain, a cross-over (γ_c) point at ~ 12.5% and ~12.1% was observed for **MeOle-CPCl** and **MeOle-CPBr** respectively, representing the breakdown of the gel network. Based on the cross-over data, MeOle-based eutectogels demonstrated higher mechanical strength in comparison to those based on MeLA and MePA, as highlighted in Table S2. This discrepancy in mechanical properties can be ascribed to the structural unsaturation in oleic acid, which enhances hydrophobicity, thereby promoting increased hydrophobic interactions within the eutectogel matrix. Consequently, this accelerates gelation (*vide supra*, Fig. 3) and contributes to the formation of a mechanically strong gel as compared to other investigated systems.

3.3. Adhesive property of the eutectogel

The studied eutectogels could be a promising candidate for TDD as the system comprises skin PEs, facilitating the penetration of drugs through the stratum corneum layer upon application to the skin (*vide infra*), thereby enabling targeted drug release at the desired site. Consequently, the drug delivery vehicle must possess adhesive properties, which play a pivotal role in TDD. With this in mind, we conducted an investigation into the adhesive capabilities of a representative eutectogel (**MeOle-CPBr**) across various surfaces, including skin, glass, plastic, and aluminum. The findings, visually shown in Fig. 6a, offer valuable insights into the adhesive behavior of the eutectogel. Moreover, we performed a lap shear displacement test to evaluate the adhesive strength of the eutectogel on different surfaces, namely glass, skin, and rubber. A consistent contact area of 15 mm was maintained between the eutectogel and each specific surface. During the test, the eutectogel was subjected to controlled stretching at a rate of 100 mm min^{-1} while the surface remained fixed. As shown in Fig. 6b, the eutectogel exhibited the highest adhesion strength on rubber (8.65 kPa), owing to the rubber's flexible, deformable, and viscoelastic nature, which increases surface conformity and contact area, thereby enhancing adhesion.[41] The adhesion strength on skin was slightly lower (7.98 kPa), likely due to variations in texture and moisture that affect its mechanical properties. In contrast, the lowest adhesion (7.21 kPa) was observed on glass, whose rigid, smooth surface limits contact area and mechanical interlocking.[42]

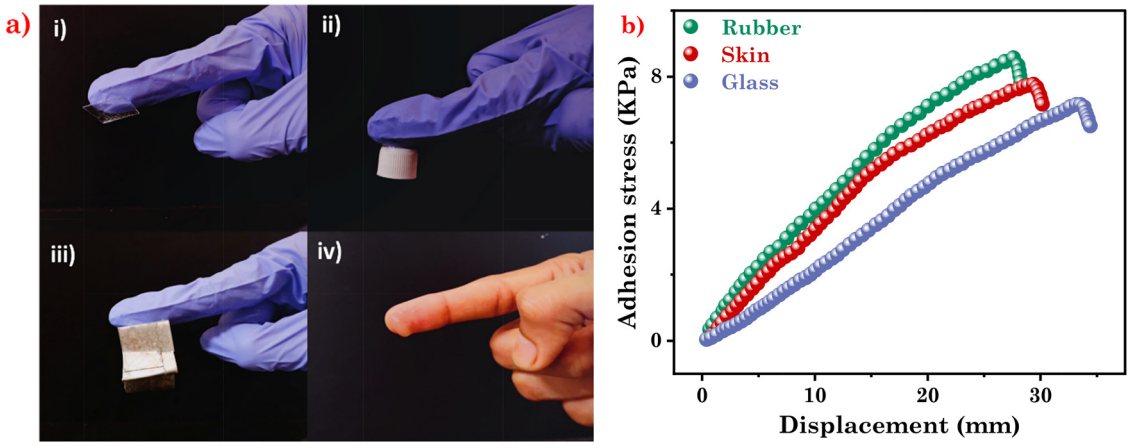

Fig. 6 (a) Adhesion of the eutectogel with (i) glass, (ii) plastic, (iii) aluminium and (iv) skin; and (b) shear stress–displacement profile of the eutectogel with different substrates.

3.4. Curcumin loading and stability within the eutectogel

We next examined the incorporation of curcumin into eutectogels. Despite its broad pharmacological potential, curcumin suffers from poor solubility, low bioavailability, and instability in aqueous or alkaline environments, which limits its clinical utility. Encapsulation within eutectogels offers a strategy to enhance curcumin's stability and delivery efficacy. Accordingly, curcumin was loaded into eutectogels prepared from THDESs composed of Mth and three different HBDs (Table 1), using the procedure described in the Experimental section. Loading varied slightly between eutectogels and increased with HBD chain length (LA < PA < Ole), consistent with greater hydrophobicity. The quantified drug loading capacity, expressed as the mass concentration of curcumin in the eutectogel, was then compared to the reported solubility of curcumin in water, which is shown to be 0.0006 mg g^{-1} in the literature.[43] This led to the calculation of the solubility advantage of the investigated systems, defined as the ratio of curcumin solubility in eutectogels to that in aqueous solution. The resulting drug loading values, along with the calculated solubility advantage, are presented in Table S3. It is evident that all studied eutectogels significantly enhanced the solubility of curcumin compared to water. In particular, MeOle-based eutectogels were found to be the most successful in terms of solubility increase; the drug loading capacity of curcumin was found to be 19.4 mg mL^{-1} (**MeOle-CPCl**) and 19.7 mg mL^{-1} (**MeOle-CPBr**), resulting in a solubility advantage exceeding thirty thousand. Additionally, we also conducted a comparative analysis of the curcumin loaded eutectogel with other curcumin loaded DES-based systems (Table S4) to gain valuable insights into the enhanced encapsulation efficiency, highlighting its potential as an effective and reliable carrier for curcumin encapsulation.

To assess the potential of eutectogels as carriers for drug delivery, we investigated the stability of curcumin when encapsulated within the eutectogel. Consequently, we placed curcumin loaded eutectogels in a dark environment at room temperature for a period of 30 days. To draw a comparison, curcumin was also dissolved in water based on its solubility

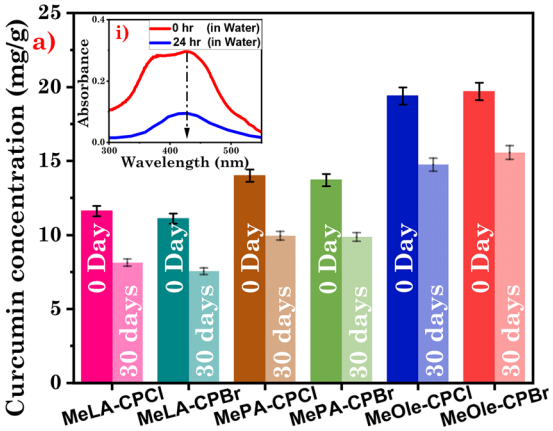

Fig. 7 Curcumin degradation in each eutectogel.

and subjected to the same environmental conditions. The concentration of curcumin was subsequently measured using UV-Vis absorbance before and after the 30-day period. It is worth mentioning that curcumin exhibited sustained stability within the eutectogels, as evidenced by the absence of any significant change in the curcumin peak at 423 nm after 30 days (Fig. S3a–f). In contrast, we observed a degradation of only 20–30% (Fig. 7a) in the eutectogel system, in comparison to the approximately 90% degradation (Fig. 7a(i)) observed in water within a mere 24-hour period. This finding underscores the extended stability of curcumin within the eutectogels, suggesting its potential as an effective means for sustained drug delivery.

3.5. Drug permeation study

Permeation studies were conducted to evaluate the transdermal delivery potential of curcumin-loaded eutectogels using goat ear pinna skin in a Franz diffusion cell. All gels contained an equivalent curcumin concentration of 500 μg g^{-1} and were tested at pH 7.4 and 32 ± 1 °C. Fig. 8 shows the cumulative permeation profiles of curcumin from all gel formulations over

48 h. To quantify skin permeation, the flux (J) and permeability coefficient (K_p) were calculated from the linear portion of the cumulative permeation curves, and the results are summarized in Table S5. MeLA-based eutectogels showed lower flux and permeability, whereas MePA- and MeOle-based eutectogels exhibited increasing flux and permeability coefficients. The enhanced permeation observed in MeOle-based eutectogels relative to MeLA-based gels aligns with previous findings reported by M. Goto, where IL[Lev][Ole] demonstrated improved drug penetration compared to IL[Lev][Lau]. This effect can be attributed to the increasing hydrophobicity of DES-based eutectogels with the increasing chain length of FAs, which leads to an increase in their interaction with the lipid-rich stratum corneum, and the presence of penetration enhancers such as menthol (HBA), FAs (HBDs: lauric acid, palmitic acid, oleic acid), and gelators (CPCl, CPBr) that disrupt stratum corneum lipids. Overall, the systematic increase in flux and K_p across the eutectogels highlights the importance of eutectogel composition in modulating curcumin permeation. MeOle-based eutectogels, with higher hydrophobicity, exhibited the most efficient transdermal delivery, suggesting their potential as a superior platform for hydrophobic drug delivery. The findings, supported by Table S5 and Fig. 8, highlight the enhanced curcumin permeation through eutectogels, with a flux of 103–115 μg cm^{-2} h^{-1}. This is markedly higher than that achieved by conventional carriers, such as liposomes (1.45 ± 0.31 μg cm^{-2} h^{-1}),[44] curcumin membranes with or without the bio-enhancer piperine (4.29 ± 1.70 and 8.10 ± 1.51 μg cm^{-2} h^{-1}, respectively),[45] and optimized nanoemulsions (1.699 ± 0.050 μg cm^{-2} h^{-1}).[46] The superior flux indicates that the DES-based eutectogel, acting as both solvent and permeation enhancer, is an efficient delivery platform. These results provide a strong basis for further mechanistic studies to understand interactions between eutectogel components and skin lipids.

3.6. Permeation mechanism

ATR-FTIR spectroscopy is a noninvasive tool that detects changes in the molecular environment of skin components by monitoring functional group vibrations in the SC layer.[47] In our study, we focused our spectral analysis on vibrations related to SC lipids and keratins. Previous research has shown that the asymmetric CH_2 stretching (ν_aCH_2) vibration and symmetric CH_2 stretching (ν_sCH_2) vibration can offer insights into the organization of lipids, including ceramides, cholesterol, and free fatty acids.[48] An increase in vibrational frequency indicates an increase in lipid disordering.[47] Fig. 9a–f and Fig. S4a–f depict the FTIR spectra of untreated skin (control) and skin post-treatment with each eutectogel. To facilitate comparison between control and treated skin samples, spectra were subjected to Gaussian deconvolution and curve fitting using Origin 2023 software.[49] Table 3 outlines the Gaussian bands representing characteristic regions of control skin and skin treated with eutectogels. In the control skin, absorption bands of ν_aCH_2 and ν_sCH_2 were observed near 2928.06 cm^{-1} and 2853.00 cm^{-1}, respectively. However, a slight increase in frequency for ν_aCH_2 and ν_sCH_2 was noted post-treatment with eutectogels, suggesting a tendency of the studied eutectogels to increase lipid disorder packing.[48] Furthermore, it is evident that treatment with eutectogels results in a noticeable decrease in the height and area of ν_aCH_2 and ν_sCH_2 peaks, indicative of reduced skin lipid content. Notably, the observed shift in the peak and the decrease in intensity follow the order MeLA < MePA < MeOle, correlating with the increasing hydrophobicity of the system due to the presence of fatty acids LA, PA, and Ole, respectively, with increasing alkyl chain length in their structures. Previous studies have highlighted that lipids in the SC organize into two dense lamellar phases with a periodicity of around 6 and 13 nm, a critical structural arrangement contributing to the barrier function of skin.[50] Our findings suggest that eutectogels may act as lipid extractors, potentially compromising the integrity of the skin barrier and thereby enhancing the permeability of drugs through the skin.

The amide I (νC═O) and amide II (νN–H) bands reveal keratin secondary structures, with amide I sensitive to α-helix and β-sheet changes.[51] Notably, skin samples treated with eutectogels exhibit a higher frequency shift in the amide I band compared to the control group, with a slightly higher shift also observed in the amide II band. Generally, weaker hydrogen bonding leads to an upward frequency shift, whereas stronger hydrogen bonding results in a downward shift.[52] Thus, alterations in the keratin configuration likely stem from the formation of hydrogen bonds with the eutectogel, potentially leading to looser heterodimers, tetramers, or higher-order keratin assemblies. This aligns with the impact of the lappaconitine-cinnamic acid ion pair complex on skin keratins.[52] It has been established that drug permeation across the SC occurs *via* transcellular, intercellular, and follicular routes (Fig. 9i). We posit that the permeation-enhancing effect of studied eutectogels could be attributed to lipid extraction and conformational changes in keratin.

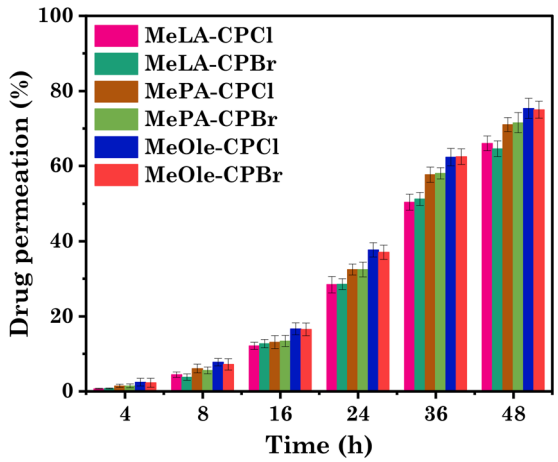

Fig. 8 *In vitro* curcumin permeation study through goat skin for each eutectogel.

3.7. *In vitro* cytotoxicity of eutectogels

The biocompatibility of the investigated eutectogels was evaluated utilizing the human immortalized keratinocyte cell line (HaCaT). With increasing concentration and particularly at a

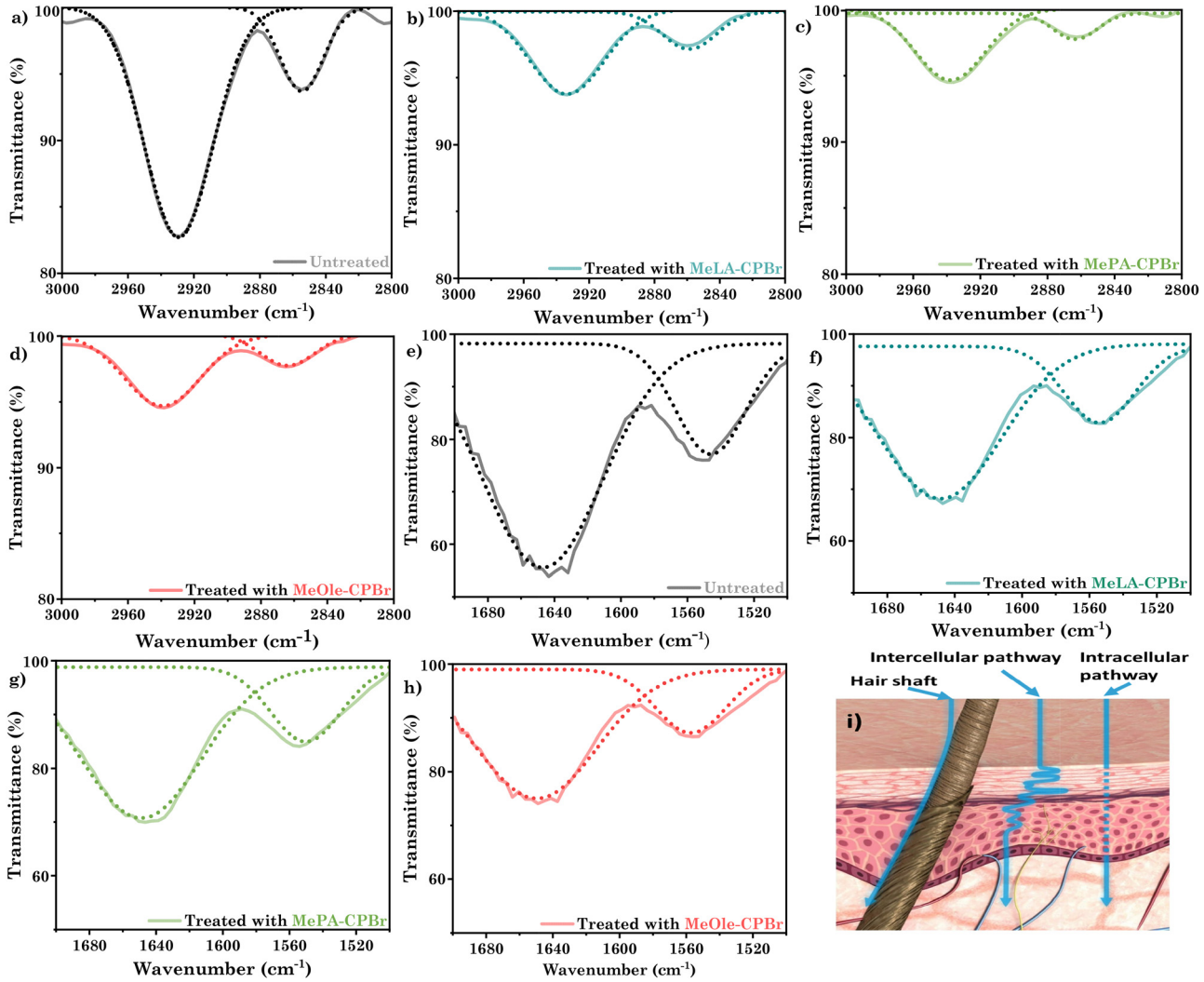

Fig. 9 (a) and (e) FTIR spectra (solid line) of untreated skin (control); (b)–(d) and (f)–(h) FTIR spectra (solid line) of skin treated with **MeLA-CPCl**, **MePA-CPCl**, and **MeOle-CPCl**, respectively. Deconvoluted FTIR spectra (dotted lines) highlight regions corresponding to lipids (a)–(d) and proteins (e)–(h). Changes in lipid content ($\nu_a CH_2$ and $\nu_s CH_2$) and protein content ($\nu C{=}O$ and $\delta N{-}H$) were analyzed based on the peak area. (i) Schematic illustration of the different drug permeation pathways through the stratum corneum (SC) layer of the skin.

Table 3 The Gaussian bands represent characteristic regions of lipids and proteins for untreated skin and skin treated with eutectogels

	Untreated skin	Treated skin					
		MeLA		MePA		MeOle	
		CPCl	CPBr	CPCl	CPBr	CPCl	CPBr
$\nu_a CH_2$	2928.06	2930.74	2933.42	2938.56	2938.51	2942.27	2939.54
$\nu_s CH_2$	2853.00	2856.32	2858.26	2859.25	2860.21	2867.21	2844.27
$\nu C{=}O$	1643.21	1646.11	1646.96	1647.71	1647.00	1646.30	1648.00
$\delta N{-}H$	1549.65	1550.34	1551.51	1550.31	1552.25	1552.41	1553.44

high concentration (10 mg mL^{-1}), each eutectogel demonstrated remarkable cell viability. Specifically, **MeLA-CPCl**, **MeLA-CPBr**, **MePA-CPCl**, **MePA-CPBr**, **MeOle-CPCl** and **MeOle-CPBr** exhibited a cell viability of ~ 96%, ~94%, ~95%, ~94%, ~93%, and ~92%, respectively, as illustrated in Fig. 10a and 11(i–vii). These results indicate the biocompatibility of the THDES-based eutectogels, thereby making them attractive candidates for applications in drug delivery and tissue engineering.

Furthermore, we employed the A431 cell lines to assess the cytotoxicity of the studied THDES-based eutectogels with and without curcumin. The drug-free eutectogels exhibited low-to-no toxicity, whereas the curcumin-loaded eutectogels displayed higher toxicity, as illustrated in Fig. 10b and 11 and 12. Hence,

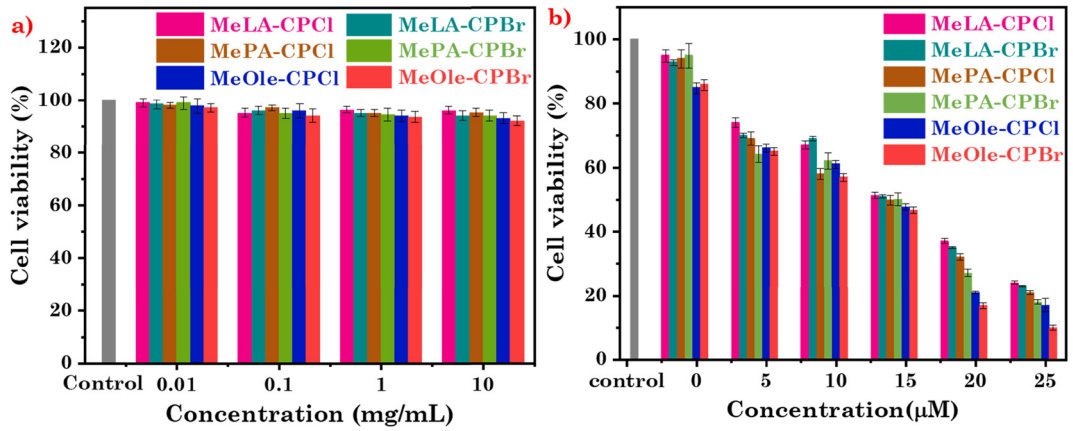

Fig. 10 Cell viability (%) of the (a) HaCAT cell line and (b) A431 cell line for each eutectogel.

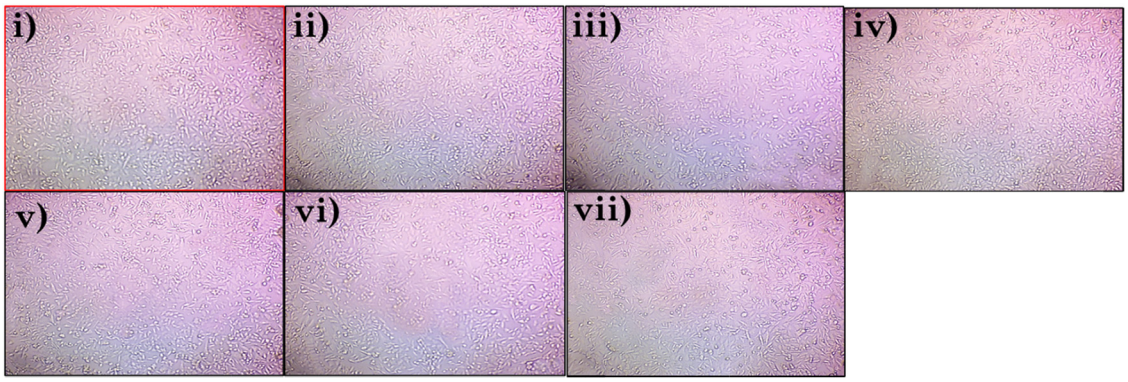

Fig. 11 Microscopic image of HaCAT cells (i) before treatment (control) and after treatment with (ii) **MeLA-CPCl**, (iii) **MeLA-CPBr**, (iv) **MePA-CPCl**, (v) **MePA-CPBr**, (vi) **MeOle-CPCl** and (vii) **MeOle-CPBr** (20× magnification; scale bar = 100 μm).

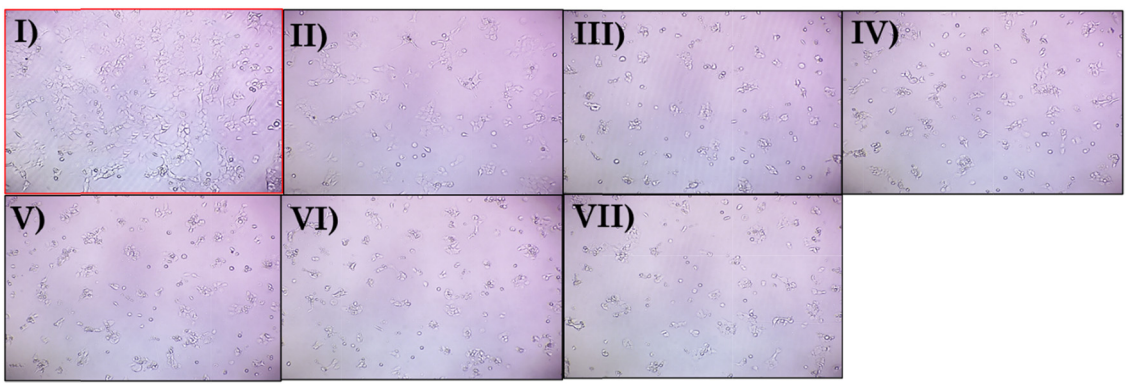

Fig. 12 Microscopic image of the A431 cell line (I) before treatment (control) and after treatment with drug loaded eutectogel (II) **MeLA-CPCl**, (III) **MeLA-CPBr**, (IV) **MePA-CPCl**, (V) **MePA-CPBr**, (VI) **MeOle-CPCl** and (VII) **MeOle-CPBr** (20× magnification; scale bar = 100 μm).

any observed cytotoxicity in the A431 cell line can be attributed to the drug rather than the eutectogels, affirming the safety of THDES-based eutectogels as a drug delivery vehicle. Additionally, we determined the IC_{50} values for the curcumin-loaded eutectogels against the A431 cell line, with the results summarized in Table S6. These findings indicate that the eutectogel without curcumin is nontoxic, and the addition of curcumin increases its efficiency in killing cancerous cells. However, further studies are needed to evaluate the efficacy and safety of this approach *in vivo*, and these data are useful for such studies.

3.8. Skin irritation test

Furthermore, assessing skin safety is essential for any transdermal drug carrier, as irritation depends on formulation,

Table 4 Skin compatibility of the volunteers 24, 48, and 72 h after the application of the studied eutectogels

System	Volunteer	Skin irritation response (24–72 h)
MeLA-CPBr	2	None
MePA-CPBr	2	None
MeOle-CPBr	2	None

concentration, absorption, dose, and skin condition, making a compatibility study crucial for first human exposure. In this study, drug-loaded eutectogels from each THDES (*i.e.*, **MeLA-CPBr**, **MePA-CPBr**, and **MeOle-CPBr** gels) were selected as representative samples to assess their skin irritability on human volunteers through the primary skin irritation test[37,38] as described in the methods section. As shown in Table 4, all eutectogels demonstrated skin biocompatibility (reaction grade 0), with no irritation observed at 24, 48, and 72 h post-treatment. While the primary irritation test conducted here only assesses the acute irritation potential of the material, these findings serve as an important preliminary step in the risk assessment process. Further studies, including long-term human trials, are required to fully evaluate the safety of prolonged skin exposure. Nevertheless, these results provide a foundation for the continued development of safe, skin-compatible drug delivery systems.

4. Conclusions

We have successfully developed a supramolecular eutectogel based on THDESs by incorporating the surfactants CPCl and CPBr, which we confirmed through FTIR analysis. This eutectogel exhibits stimuli-responsive behavior, particularly to temperature variations, which was investigated through UV-vis spectroscopy to monitor the opacity of the eutectogel as a function of temperature. Employing SEM, we examined the morphology of the gels and evaluated their adhesive properties through lap-shear testing. Further investigation into the ability of the eutectogels to encapsulate the model drug curcumin revealed remarkable loading capacities, with ~30 000 times more curcumin in the MeOle-based system, ~23 000 times more in the MePA-based system, and ~18 000 times more in the MeLA-based system compared to water. Additionally, *ex vivo* experiments, including Franz diffusion cell tests and FTIR analysis on skin, were conducted to assess drug permeation and confirm its impact on skin structure and penetration through the stratum corneum. We also evaluated their biocompatibility through a primary skin irritation test and tested their cytotoxicity using the HaCaT cell line, along with the investigation of their effects on the A431 cell line. The results were promising, supporting the potential use of the studied supramolecular eutectogels in transdermal drug delivery systems (TDDSs). Although this study focuses on curcumin, the formulation strategy and findings establish a platform technology that could be extended to other hydrophobic drugs for transdermal delivery in future work. These results allow us to conclude that the supramolecular eutectogels developed here could potentially be biocompatible, non-irritating, and suitable for use in TDD systems as PEs, opening the possibility to apply these materials for delivering drugs with low skin permeation capacity.

List of abbreviations

THDES	Therapeutic hydrophobic deep eutectic solvent
TDD	Transdermal drug delivery
CPCl	Cetyl-pyridinium chloride
CPBr	Cetyl-pyridinium bromide
Mth	Menthol
FAs	Fatty acids
LA	Lauric acid
PA	Palmitic acid
Ole	Oleic acid
MeLA	Menthol + lauric acid - DES
MePA	Menthol + palmitic acid - DES
MeOle	Menthol + oleic acid – DES
ILs	Ionic liquids
DESs	Deep eutectic solvents
TDES	Therapeutic deep eutectic solvent
HBA	Hydrogen bond acceptor
HBD	Hydrogen bond donor

Author contributions

Nildhara Parsana: conceptualization, methodology, writing – original draft and visualization. Priyam Patel: conceptualization, methodology, and visualization. Hiral Ukani: conceptualization, methodology, and visualization. Sugam Kumar: conceptualization and methodology. Vinod K Aswal: conceptualization and methodology. Omar A. El Seoud: writing – original draft and visualization. Naved I Malek: conceptualization, supervision, writing – review and editing, and funding acquisition. All authors have given approval to the final version of the manuscript.

Conflicts of interest

There are no conflicts to declare.

Data availability

Data will be made available on request.

Supplementary information (SI): criteria for the evaluation of the primary irritation test, FTIR spectra of pure components, DESs and their gel, transition temperatures (gel to sol) for all the eutectogels, rheological crossover data of eutectogels, curcumin encapsulation within eutectogels, comparative curcumin encapsulation with other reported systems, curcumin degradation within eutectogels, curcumin permeation through skin using FTIR, and IC_{50} value of curcumin loaded eutectogels against the A431 cell line (PDF), and a video of gel-sol-gel transition (AVI). See DOI: **https://doi.org/10.1039/d5tb01470k**.

Acknowledgements

NM and SK acknowledge the financial assistance from UGC-DAE-CSR for the Collaborative Research Scheme (UDCSR/MUM/AO/CRS-M-997/2023). IP and NM acknowledge financial assistance from the Student Start-up and Innovation Policy, Gujarat State-wide Project Number SVNIT/ASHINE/SSIP 2.0/IGNITION 3.0/2023-24/113. OAS thanks CNPq (grants 306108/2019-4; 141853/2019-0) and FAPESP (grant 2014/22136-4) for the grants.

References

1 P. Basnet and N. Skalko-Basnet, Curcumin: An Anti-Inflammatory Molecule from a Curry Spice on the Path to Cancer Treatment, *Molecules*, 2011, **16**(6), 4567–4598, DOI: 10.3390/molecules16064567.

2 Y. Sugiyama, S. Kawakishi and T. Osawa, Involvement of the β-Diketone Moiety in the Antioxidative Mechanism of Tetrahydrocurcumin, *Biochem. Pharmacol.*, 1996, **52**(4), 519–525, DOI: 10.1016/0006-2952(96)00302-4.

3 Y. Wang, Y. Shi, X. Xu, F. Liu, H. Yao, G. Zhai, J. Hao and G. Li, Preparation of PANI-Coated Poly (Styrene-Co-Styrene Sulfonate) Nanoparticles in Microemulsion Media, *Colloids Surf., A*, 2009, **345**(1–3), 71–74, DOI: 10.1016/j.colsurfa.2009.04.029.

4 T. Zhang, Y. Chen, Y. Ge, Y. Hu, M. Li and Y. Jin, Inhalation Treatment of Primary Lung Cancer Using Liposomal Curcumin Dry Powder Inhalers, *Acta Pharm. Sin. B*, 2018, **8**(3), 440–448, DOI: 10.1016/j.apsb.2018.03.004.

5 T. Gómez-Sierra, D. Eugenio-Pérez, A. Sánchez-Chinchillas and J. Pedraza-Chaverri, Role of Food-Derived Antioxidants against Cisplatin Induced-Nephrotoxicity, *Food Chem. Toxicol.*, 2018, **120**, 230–242, DOI: 10.1016/j.fct.2018.07.018.

6 N. Parsamanesh, M. Moossavi, A. Bahrami, A. E. Butler and A. Sahebkar, Therapeutic Potential of Curcumin in Diabetic Complications, *Pharmacol. Res.*, 2018, **136**, 181–193, DOI: 10.1016/j.phrs.2018.09.012.

7 M. V. Swamy, B. Citineni, J. M. R. Patlolla, A. Mohammed, Y. Zhang and C. V. Rao, Prevention and Treatment of Pancreatic Cancer by Curcumin in Combination With Omega-3 Fatty Acids, *Nutr. Cancer*, 2008, **60**(sup1), 81–89, DOI: 10.1080/01635580802416703.

8 S.-E. Chuang, A.-L. Cheng, J.-K. Lin and M.-L. Kuo, Inhibition by Curcumin of Diethylnitrosamine-Induced Hepatic Hyperplasia, Inflammation, Cellular Gene Products and Cell-Cycle-Related Proteins in Rats, *Food Chem. Toxicol.*, 2000, **38**(11), 991–995, DOI: 10.1016/S0278-6915(00)00101-0.

9 J. Kim, Chemopreventive Effects of Carotenoids and Curcumins on Mouse Colon Carcinogenesis after 1,2-Dimethylhydrazine Initiation, *Carcinogenesis*, 1998, **19**(1), 81–85, DOI: 10.1093/carcin/19.1.81.

10 T. Dorai, Y. Cao, B. Dorai, R. Buttyan and A. E. Katz, Therapeutic Potential of Curcumin in Human Prostate Cancer. III. Curcumin Inhibits Proliferation, Induces Apoptosis, and Inhibits Angiogenesis of LNCaP Prostate Cancer Cells in Vivo, *Prostate*, 2001, **47**(4), 293–303, DOI: 10.1002/pros.1074.

11 M. M. LoTempio, M. S. Veena, H. L. Steele, B. Ramamurthy, T. S. Ramalingam, A. N. Cohen, R. Chakrabarti, E. S. Srivatsan and M. B. Wang, Curcumin Suppresses Growth of Head and Neck Squamous Cell Carcinoma, *Clin. Cancer Res.*, 2005, **11**(19), 6994–7002, DOI: 10.1158/1078-0432.CCR-05-0301.

12 J. Odot, P. Albert, A. Carlier, M. Tarpin, J. Devy and C. Madoulet, In Vitro and in Vivo Anti-tumoral Effect of Curcumin against Melanoma Cells, *Int. J. Cancer*, 2004, **111**(3), 381–387, DOI: 10.1002/ijc.20160.

13 M. Cruz–Correa, D. A. Shoskes, P. Sanchez, R. Zhao, L. M. Hylind, S. D. Wexner and F. M. Giardiello, Combination Treatment With Curcumin and Quercetin of Adenomas in Familial Adenomatous Polyposis, *Clin. Gastroenterol. Hepatol.*, 2006, **4**(8), 1035–1038, DOI: 10.1016/j.cgh.2006.03.020.

14 R. A. Sharma, S. A. Euden, S. L. Platton, D. N. Cooke, A. Shafayat, H. R. Hewitt, T. H. Marczylo, B. Morgan, D. Hemingway, S. M. Plummer, M. Pirmohamed, A. J. Gescher and W. P. Steward, Phase I Clinical Trial of Oral Curcumin, *Clin. Cancer Res.*, 2004, **10**(20), 6847–6854, DOI: 10.1158/1078-0432.CCR-04-0744.

15 P. Anand, A. B. Kunnumakkara, R. A. Newman and B. B. Aggarwal, Bioavailability of Curcumin: Problems and Promises, *Mol. Pharm.*, 2007, **4**(6), 807–818, DOI: 10.1021/mp700113r.

16 N. Dhillon, B. B. Aggarwal, R. A. Newman, R. A. Wolff, A. B. Kunnumakkara, J. L. Abbruzzese, C. S. Ng, V. Badmaev and R. Kurzrock, Phase II Trial of Curcumin in Patients with Advanced Pancreatic Cancer, *Clin. Cancer Res.*, 2008, **14**(14), 4491–4499, DOI: 10.1158/1078-0432.CCR-08-0024.

17 Md. R. Chowdhury, R. M. Moshikur, R. Wakabayashi, Y. Tahara, N. Kamiya, M. Moniruzzaman and M. Goto, Development of a Novel Ionic Liquid–Curcumin Complex to Enhance Its Solubility, Stability, and Activity, *Chem. Commun.*, 2019, **55**(54), 7737–7740, DOI: 10.1039/C9CC02812A.

18 N. Parsana, H. Ukani, D. S. Chauhan, O. El Seoud, S. Mehra, A. Kumar, N. Raje and N. Malek, Biocompatible, Injectable and Self-Healable MOF-Based Anti-Freezing Eutectogels for Higher Encapsulation and Sustained Release of the Anticancer Drug Curcumin, *RSC Pharm.*, 2024, **1**(2), 317–332, DOI: 10.1039/D3PM00088E.

19 T. Jeliński, M. Przybyłek and P. Cysewski, Natural Deep Eutectic Solvents as Agents for Improving Solubility, Stability and Delivery of Curcumin, *Pharm. Res.*, 2019, **36**(8), 116, DOI: 10.1007/s11095-019-2643-2.

20 M. L. Picchio, M. S. Orellano, M. A. Motta, C. Huck-Iriart, D. Sánchez-deAlcázar, R. López-Domene, B. Martín-García, A. Larrañaga, A. Beloqui, D. Mecerreyes and M. Calderón, Elastomeric Protein Bioactive Eutectogels for Topical Drug Delivery, *Adv. Funct. Mater.*, 2024, **34**(18), 2313747, DOI: 10.1002/adfm.202313747.

21 A. R. C. Duarte, A. S. D. Ferreira, S. Barreiros, E. Cabrita, R. L. Reis and A. Paiva, A Comparison between Pure Active

Pharmaceutical Ingredients and Therapeutic Deep Eutectic Solvents: Solubility and Permeability Studies, *Eur. J. Pharm. Biopharm.*, 2017, **114**, 296–304, DOI: 10.1016/j.ejpb.2017.02.003.

22 A. Paiva, R. Craveiro, I. Aroso, M. Martins, R. L. Reis and A. R. C. Duarte, Natural Deep Eutectic Solvents – Solvents for the 21st Century, *ACS Sustainable Chem. Eng.*, 2014, **2**(5), 1063–1071, DOI: 10.1021/sc500096j.

23 B. D. Ribeiro, C. Florindo, L. C. Iff, M. A. Z. Coelho and I. M. Marrucho, Menthol-Based Eutectic Mixtures: Hydrophobic Low Viscosity Solvents, *ACS Sustainable Chem. Eng.*, 2015, **3**(10), 2469–2477, DOI: 10.1021/acssuschemeng.5b00532.

24 T. Nakatsuji, M. C. Kao, J.-Y. Fang, C. C. Zouboulis, L. Zhang, R. L. Gallo and C.-M. Huang, Antimicrobial Property of Lauric Acid Against Propionibacterium Acnes: Its Therapeutic Potential for Inflammatory Acne Vulgaris, *J. Invest. Dermatol.*, 2009, **129**(10), 2480–2488, DOI: 10.1038/jid.2009.93.

25 A. P. Desbois and V. J. Smith, Antibacterial Free Fatty Acids: Activities, Mechanisms of Action and Biotechnological Potential, *Appl. Microbiol. Biotechnol.*, 2010, **85**(6), 1629–1642, DOI: 10.1007/s00253-009-2355-3.

26 A. Mortensen, F. Aguilar, R. Crebelli, A. Di Domenico, B. Dusemund, M. J. Frutos, P. Galtier, D. Gott, U. Gundert-Remy, J. Leblanc, O. Lindtner, P. Moldeus, P. Mosesso, D. Parent-Massin, A. Oskarsson, I. Stankovic, I. Waalkens-Berendsen, R. A. Woutersen, M. Wright, M. Younes, P. Boon, D. Chrysafidis, R. Gürtler, P. Tobback, P. Gergelova, A. M. Rincon and C. Lambré, Re-evaluation of Fatty Acids (E 570) as a Food Additive, *EFSA J.*, 2017, **15**(5), 4785, DOI: 10.2903/j.efsa.2017.4785.

27 B. Li, T. Xiao, S. Guo, Y. Wu, R. Lai, Z. Liu, W. Luo and Y. Xu, Oxymatrine-Fatty Acid Deep Eutectic Solvents as Novel Penetration Enhancers for Transdermal Drug Delivery: Formation Mechanism and Enhancing Effect, *Int. J. Pharm.*, 2023, **637**, 122880, DOI: 10.1016/j.ijpharm.2023.122880.

28 H. Ukani, Pratyush, S. Kumar, V. K. Aswal, A. A. Al-Ghamdi and N. I. Malek, Cholesterol Mediated Stable Vesicles: A Nano Drug Delivery Vehicle for Anti-cancer Drugs Curcumin and 5-Fluorourecil, *ChemistrySelect*, 2022, **7**(33), e202201613, DOI: 10.1002/slct.202201613.

29 T. Patel, R. Pansuriya, S. Mehra, A. Kumar, O. El Seoud, M. A. Assiri and N. Malek, Photo and Temperature Responsive Novel Surface Active Ionic Liquid-Based Polymeric Hydrogel, *J. Mol. Liq.*, 2023, **391**, 123099, DOI: 10.1016/j.molliq.2023.123099.

30 R. Pansuriya, S. Mehra, A. Kumar, O. El Seoud, S. Kumar Kailasa and N. Malek, Two Birds with One Stone: Multifunctional Ionic Liquid Based Polymeric Hydrogel as Decontaminant and Vehicle for Drug Delivery, *J. Mol. Liq.*, 2023, **382**, 121857, DOI: 10.1016/j.molliq.2023.121857.

31 H. Ukani, S. Mehra, B. Parmar, A. Kumar, I. Khan, O. A. El Seoud and N. Malek, Metal–Organic Framework-Based Aerogel: A Novel Adsorbent for the Efficient Removal of Heavy Metal Ions and Selective Removal of a Cationic Dye from Aqueous Solution, *Ind. Eng. Chem. Res.*, 2023, **62**(12), 5002–5014, DOI: 10.1021/acs.iecr.2c03804.

32 N. Parsana, O. El Seoud, A. Al-Ghamdi, N. Kasoju and N. Malek, Deep Eutectic Solvent and Poly (Vinyl Alcohol) Based Self-healable, Injectable and Adhesive ''Eutectogel'': An Emerging Drug Delivery Vehicle, *ChemistrySelect*, 2024, **9**(1), e202304157, DOI: 10.1002/slct.202304157.

33 N. Parsana, S. Kumar, V. K. Aswal, O. El. Seoud and N. I. Malek, Self-Healable, Injectable, and Conductive Supramolecular Eutectogel for the Encapsulation and Sustained Release of the Anticancer Drug Curcumin, *ACS Appl. Eng. Mater.*, 2023, **1**(1), 380–393, DOI: 10.1021/acsaenm.2c00095.

34 N. Parsana, H. Ukani, O. A. El Seoud, A. Al-Ghamdi and N. Malek, Deep Eutectic Solvent Based Self-Healable, Stretchable and Injectable Eutectogels: A Versatile Platform for Breast Cancer Treatment, *Chem. Eng. J.*, 2024, **488**, 150703, DOI: 10.1016/j.cej.2024.150703.

35 B. Hammouda, D. L. Ho and S. Kline, Insight into Clustering in Poly(Ethylene Oxide) Solutions, *Macromolecules*, 2004, **37**(18), 6932–6937, DOI: 10.1021/ma049623d.

36 B. Hammouda, F. Horkay and M. L. Becker, Clustering and Solvation in Poly(Acrylic Acid) Polyelectrolyte Solutions, *Macromolecules*, 2005, **38**(5), 2019–2021, DOI: 10.1021/ma047960g.

37 D. A. Basketter, M. Chamberlain, H. A. Griffiths, M. Rowson, E. Whittle and M. York, The Classification of Skin Irritants by Human Patch Test, *Food Chem. Toxicol.*, 1997, **35**(8), 845–852, DOI: 10.1016/S0278-6915(97)00053-7.

38 C. M. Batista, L. A. de Queiroz, Â. V. F. Alves, E. C. A. Reis, F. A. Santos, T. N. Castro, B. S. Lima, A. A. S. Araújo, C. A. P. Godoy, P. Severino, A. Cano, A. Santini, R. Capasso, R. L. C. de Albuquerque Júnior, J. C. Cardoso and E. B. Souto, Photoprotection and Skin Irritation Effect of Hydrogels Containing Hydroalcoholic Extract of Red Propolis: A Natural Pathway against Skin Cancer, *Heliyon*, 2022, **8**(2), e08893, DOI: 10.1016/j.heliyon.2022.e08893.

39 B. D. Ribeiro, C. Florindo, L. C. Iff, M. A. Z. Coelho and I. M. Marrucho, Menthol-Based Eutectic Mixtures: Hydrophobic Low Viscosity Solvents, *ACS Sustainable Chem. Eng.*, 2015, **3**(10), 2469–2477, DOI: 10.1021/acssuschemeng.5b00532.

40 J. E. Curtis, A. McAuley, H. Nanda and S. Krueger, Protein Structure and Interactions in the Solid State Studied by Small-Angle Neutron Scattering, *Faraday Discuss.*, 2012, **158**, 285, DOI: 10.1039/c2fd20027a.

41 M. Kuddushi, S. Rajput, A. Shah, J. Mata, V. K. Aswal, O. El Seoud, A. Kumar and N. I. Malek, Stimuli Responsive, Self-Sustainable, and Self-Healable Functionalized Hydrogel with Dual Gelation, Load-Bearing, and Dye-Absorbing Properties, *ACS Appl. Mater. Interfaces*, 2019, **11**(21), 19572–19583, DOI: 10.1021/acsami.9b01129.

42 G. Raos and B. Zappone, Polymer Adhesion: Seeking New Solutions for an Old Problem, *Macromolecules*, 2021, **54**(23), 10617–10644, DOI: 10.1021/acs.macromol.1c01182.

43 T. Jeliński, M. Przybyłek and P. Cysewski, Natural Deep Eutectic Solvents as Agents for Improving Solubility, Stability and Delivery of Curcumin, *Pharm. Res.*, 2019, **36**(8), 116, DOI: 10.1007/s11095-019-2643-2.

44 Y. Chen, Q. Wu, Z. Zhang, L. Yuan, X. Liu and L. Zhou, Preparation of Curcumin-Loaded Liposomes and Evaluation of Their Skin Permeation and Pharmacodynamics, *Molecules*, 2012, **17**(5), 5972–5987, DOI: **10.3390/molecules17055972**.

45 C. Jantarat, P. Sirathanarun, S. Boonmee, W. Meechoosin and H. Wangpittaya, Effect of Piperine on Skin Permeation of Curcumin from a Bacterially Derived Cellulose-Composite Double-Layer Membrane for Transdermal Curcumin Delivery, *Sci. Pharm.*, 2018, **86**(3), 39, DOI: **10.3390/scipharm86030039**.

46 H. Rachmawati, D. K. Budiputra and R. Mauludin, Curcumin Nanoemulsion for Transdermal Application: Formulation and Evaluation, *Drug Dev. Ind. Pharm.*, 2015, **41**(4), 560–566, DOI: **10.3109/03639045.2014.884127**.

47 L. Rubio, C. Alonso, G. Rodríguez, M. Cócera, C. López-Iglesias, L. Coderch, A. De la Maza, J. L. Parra and O. López, Bicellar Systems as New Delivery Strategy for Topical Application of Flufenamic Acid, *Int. J. Pharm.*, 2013, **444**(1–2), 60–69, DOI: **10.1016/j.ijpharm.2013.01.034**.

48 D. Yang, C. Liu, D. Ding, P. Quan and L. Fang, The Molecular Design of Drug-Ionic Liquids for Transdermal Drug Delivery: Mechanistic Study of Counterions Structure on Complex Formation and Skin Permeation, *Int. J. Pharm.*, 2021, **602**, 120560, DOI: **10.1016/j.ijpharm.2021.120560**.

49 A. Banerjee, K. Ibsen, Y. Iwao, M. Zakrewsky and S. Mitragotri, Transdermal Protein Delivery Using Choline and Geranate (CAGE) Deep Eutectic Solvent, *Adv. Healthcare Mater.*, 2017, **6**(15), 1601411, DOI: **10.1002/adhm.201601411**.

50 T. Marjukka Suhonen, A. J. Bouwstra and A. Urtti, Chemical Enhancement of Percutaneous Absorption in Relation to Stratum Corneum Structural Alterations, *J. Controlled Release*, 1999, **59**(2), 149–161, DOI: **10.1016/S0168-3659(98)00187-4**.

51 Q. Tian, P. Quan, L. Fang, H. Xu and C. Liu, A Molecular Mechanism Investigation of the Transdermal/Topical Absorption Classification System on the Basis of Drug Skin Permeation and Skin Retention, *Int. J. Pharm.*, 2021, **608**, 121082, DOI: **10.1016/j.ijpharm.2021.121082**.

52 M. Li, C. Liu, Y. Cai, H. Song and L. Fang, Transdermal Enhancement Strategy of Lappaconitine: Alteration of Keratin Configuration by Counter-Ion, *AAPS PharmSciTech*, 2022, **23**(1), 61, DOI: **10.1208/s12249-021-02190-9**.